Installing Guest Molecules at Specific Sites Within Scaffold Protein Crystals

Thaddaus R. Huber, Eli C. McPherson, Carolyn E. Keating, Christopher D. Snow*

†*Department of Chemical and Biological Engineering, Colorado State University, 1301 Campus Delivery*
Fort Collins, Colorado 80523, USA
E-mail: Christopher.Snow@colostate.edu

Abstract: Protein crystals are porous self-assembling materials that can be rapidly evolved by mutagenesis. We aimed to develop scaffold assisted crystallography techniques in an engineered protein crystal with large pores (>13 nm). Guest molecules were installed via a single covalent bond to attempt to reduce the conformational freedom and achieve high occupancy structures. We used 4 different conjugation strategies to attach guest molecules to 3 different cysteine sites within pre-existing protein crystals. In all but one case, the presence of the adduct was obvious in the electron density. Structure determination of larger guest molecules may be feasible due to the large pores of the engineered scaffold crystals.

Precise position control of functional molecules in 3-dimensions will result in materials with unprecedented performance for diverse applications including biosensing, catalysis, energy conversion, biomedicine, and biotechnology. Researchers have repurposed diverse natural self-assembled architectures including oligomers, fibers[1–4], cages[5–11], capsids[12–14], 2-D S-layers[15–17], and protein crystals[18–23] in pursuit of nanotechnology applications. Protein crystals are highly porous materials and x-ray diffraction (XRD) can elucidate the resulting atomic structure. Thus, we hypothesized that protein crystals could be a favorable platform for scaffold-assisted structure determination.

By soaking small molecules into metal organic frameworks (MOFs), Fujita and coworkers developed the "crystalline sponge" method for host-guest crystallographic structure determination.[24] This method relies on adventitious, non-covalent interactions to adsorb and order guest molecules.[25] We hypothesized that guest molecule installation via a single covalent bond might sufficiently reduce the conformational freedom to provide a feasible alternative approach for scaffold-assisted crystallography. Recent work by Yaghi and coworkers supports this idea, with their successful structure determination of various guest molecules covalently attached in a MOF.[26] Thus, we aimed to engineer unique capture sites for covalent installation of molecules in a protein crystal.

One hypothetical barrier would be a lack of protein crystal plasticity; changes to the constituent monomers could disrupt crystallization or reduce crystal quality.[27,28] Previous successes in functionalizing protein crystals have relied upon modification of the protein prior to crystallization,[29] which can alter or abrogate crystallization. Even trace labeling protein monomers with fluorophores (<10 mol%) can disrupt crystal nucleation.[30] The approach demonstrated herein decouples crystallization from subsequent modification steps. We first prepare porous scaffold crystal variants that present cysteine proximal to large solvent channels and subsequently install small molecules at these sites. The resulting modified crystalline scaffolds can then be validated using XRD. By performing asynchronous crystallization and covalent small molecule installation, we demonstrate unprecedented control over molecule position in three-dimensional space.

Results

In previous work, we engineered a putative periplasmic polyisoprenoid-binding protein from Campylobacter jejuni (CJ) that crystallized with large (13 nm) solvent channels. We demonstrated that CJ crystals could selectively bind gold nanoparticles or fluorescent

proteins.[31,32] Here, solvent exposed residues on the surface of the CJ axial pores were individually mutated to cysteine. These "installation sites" were selected to maximize the inter-site distance between symmetry copies throughout the crystal (Figure 1). Thus, each installed guest molecule will experience symmetry-equivalent interactions with neighboring amino acids and can independently adopt a preferred conformation.

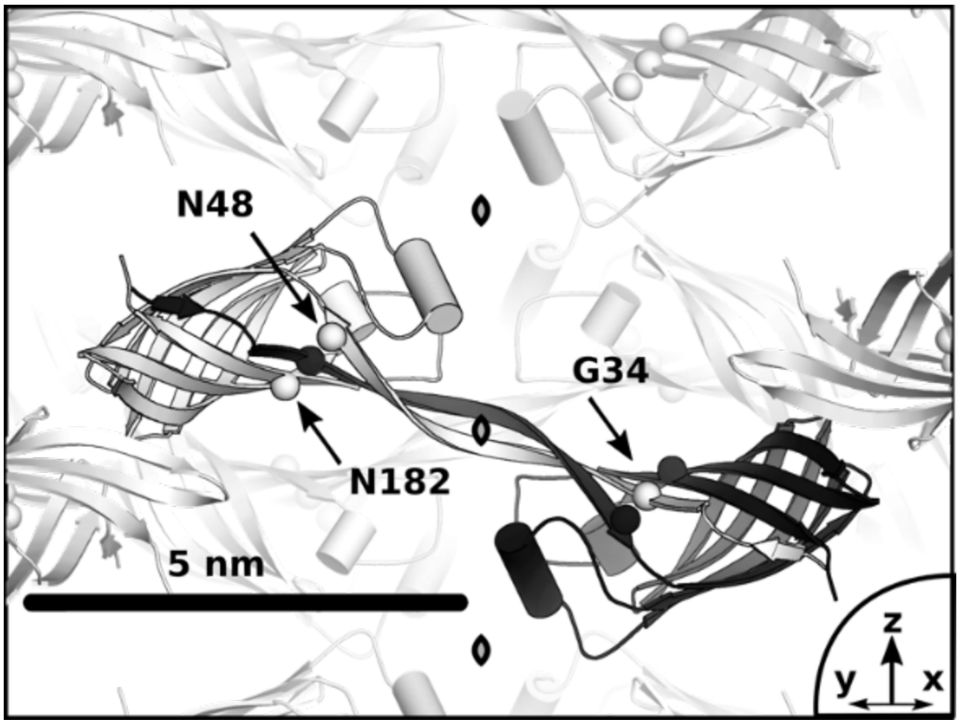

Figure 1. Candidate thiol mutation sites (spheres) were selected for maximal inter-site distance and accessibility to the large axial pore (~13 nm). A cleft on the nanopore surface presented three candidate mutation sites, G34C, N48C, N182C. One domain swapped dimer is accentuated (black and white), and 3 proximal 2-fold symmetry axes are marked (curved diamonds). The distance to the nearest symmetry mutation is 42.2 Å, 45.9 Å, and 46.3 Å for G34C, N48C, and N182C respectively.

Chemical conjugation via engineered surface cysteine residues is appealing due to the absence of cysteine residues in wild-type CJ crystals (Figure S1) and the diverse, established chemistry for thiol conjugation.[33] While cysteine mutations might, in principle, alter or abrogate crystallization, we readily obtained the expected P622 crystals for three variants: G34C, N48C, and N182C (Figure 2b, h, and n and Figures S2-S4 and Table S1).

Solvent channels within protein crystals are used in classical protein crystallography for diffusion of heavy atoms for protein crystal phasing.[34] To this end, mercury derivatives are useful due the strong propensity of thiols to covalently bind mercury (Figure S5).[35] To demonstrate engineered thiol accessibility, CJ cysteine mutant crystals were exposed to hydroxymercuribenzoate (MBO), and XRD was subsequently performed. Obvious electron density features were observed for all three cysteine-variants (Figure 2c, i, and o). MBO ligand was fit with 85% occupancy for N48C and 90% occupancy for G34C. The electron density suggested clear directionality for the benzoic acid group for the N48C adduct, but not for G34C. N182C had an extended electron density feature suggesting multiple states and was fit with two 50%-occupancy states (Figure 2o).

Free thiols can be oxidized to mixed disulfides via disulfide exchange reactions (Figure S6).[33] Ellman's reagent, 5,5'-dithio-bis(2-nitrobenzoic acid) (DTNB), a compound useful for the quantitative determination of sulfhydryls, was selected as a target chromogenic

reagent to demonstrate disulfide exchange on the crystal.[36–38] Addition of DTNB to CJ variants in solution proceeded to near completion as confirmed by absorbance at 412 nm (Figure S7). When CJ cysteine mutant crystals were exposed to DTNB, the crystals temporarily acquired a faint yellow hue before the reaction product 5-thio-2-nitrobenzoic acid (TNB^{-2}) could diffuse out of the crystals. After washing the crystals to remove excess DTNB and TNB^{-2}, an intense yellow dye release could be triggered for all three cysteine variant crystals by adding 20 μL of 10 mM 2-mercaptoethanol (BME) (Figure S8). XRD diffraction elucidated a single conformation for installed 5-mercapto-2-nitro-benzoic acid (MNB) ligand on all three cysteine variants at 100% occupancy (Figures 2d, j, and p).

Thiols can also undergo rapid interchange reactions with diselenide compounds[39,40] to form mixed thiol-selenide compounds (Figure S9). After incubation with selenocystine, XRD revealed modifications on all three cysteine variants indicative of selenocysteine (SEC) installation (Figures 2e, k, and q). SEC ligand could be fit to two conformations at 50% occupancy for G34C and a single 90%-occupancy conformation for N48C. Beyond the heavy selenium atom, the rest of the conjugate was not obvious for both variants. While the S-Se bond formation appears to have a preferred geometry (±90° dihedral), the rest of the conjugate has free rotatable bonds leading to disorder. SEC installation at N182C better resolved the conjugate conformation, with a single state at 100% occupancy (Figure 2q).

Haloalkyl derivatives are some of the most widely used conjugates for modifying thiols. The nucleophilic thiolate of the protein reacts with the halogenated alkyl via an SN2 reaction forming a stable thioether linkage (Figure S10). Due to its fluorogenic properties, monobromobimane (mBBr) ($\lambda_{exc}/\lambda_{em}$=394/490), was selected as the target reagent for demonstrating halo-alkyl installation.[41] mBBr is essentially non-fluorescent until conjugated to a thiol. CJ cysteine-bearing crystals were exposed to mBBr and the fluorescence was monitored via confocal microscopy. Only crystals containing thiol mutations were fluorescent above background (Figure S11). XRD was performed on the resulting crystals and installation was observed on N48C and N182C. Bimane adducts (MBB) were fit to single conformations for N48C and N182C at 100% and 90% occupancy respectively (Figure 2l and r).

We have confirmed multiple types of post-crystallization conjugation chemistry at multiple sites on a protein. The XRD results are summarized in Table 1 (for full x-ray statistics see Table S1-S5 and Figure S14). Reaction yields sufficient for high occupancy installation were achieved despite the high salt environment required for preserving protein crystal integrity. To validate the standard $2mF_o$-DF_c maps (Figure 2) we compared them (Figures S15, S16, and S17) to discovery maps,[42] FEM maps,[43] Polder omit maps,[44] and classical simulated annealing omit maps.[45] Real space correlation coefficient values from the $2mF_o$-DF_c maps were calculated for each installed guest molecule using Phenix.[46]

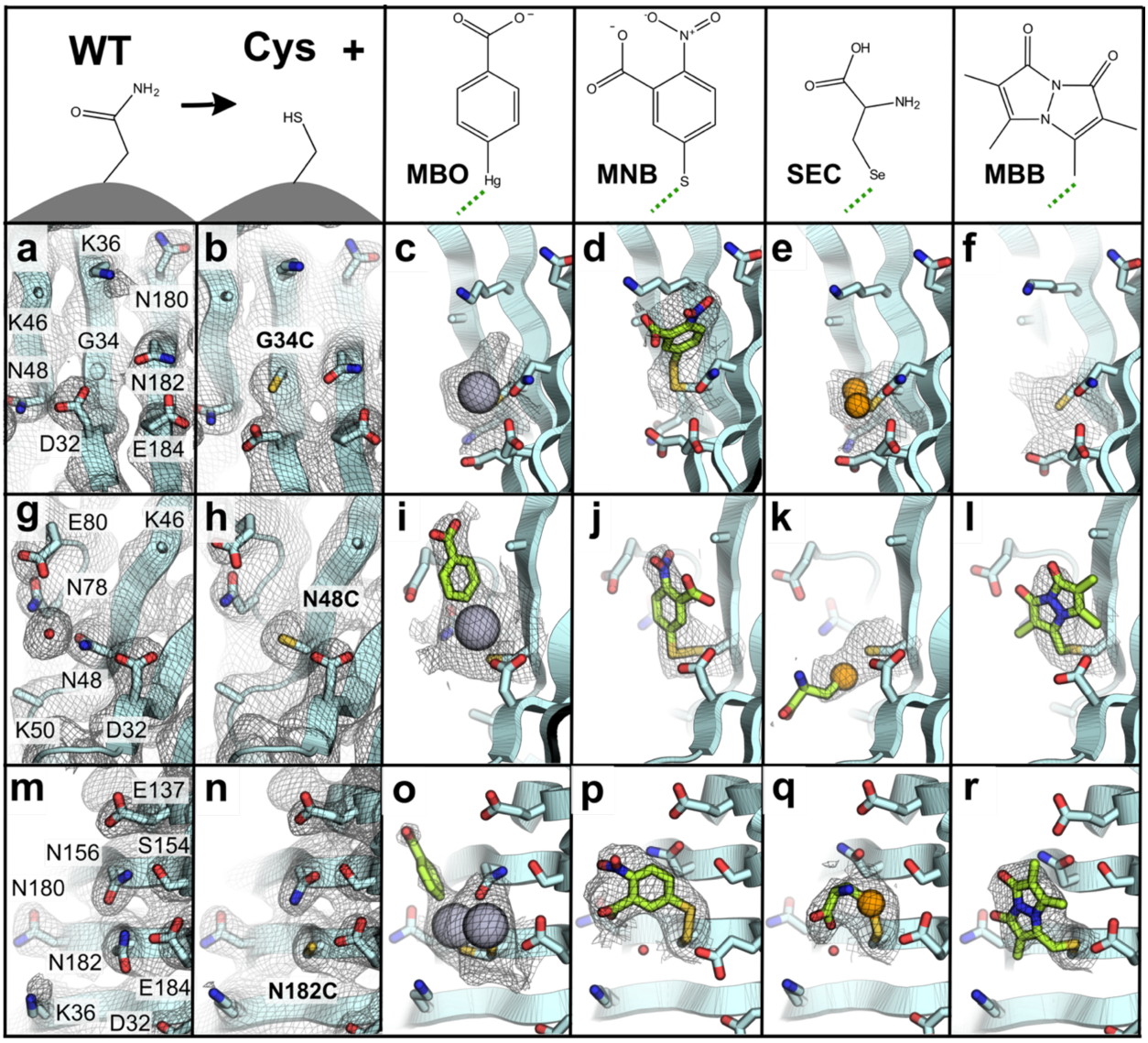

Figure 2. 2mFo-DFc maps contoured to 0.8 σ for (a) CJ wild-type (G34 alpha carbon marked with a sphere) and (b) G34C. After installa-tion at G34C: (c) One 90%-occupancy mercury position for 2-hydroxymercuribenzoic acid (MBO) (d) One 100%-occupancy conformation for 5-mercapto-2-nitro-benzoic acid (MNB). (e) For selenocysteine (SEC), two 50%-occupancy selenium positions (f) The electron density was insufficient to place the bimane adduct (MNB); (g) CJ wild-type centered at N48 and (h) N48C. After installation at N48C: (i) One 85%-occupancy conformation for MBO. (j) One 100%-occupancy conformation for MNB. (k) One 90%-occupancy conformation for SEC was modeled, though part of the flexible adduct was not resolved. (l) One 100%-occupancy conformation for MBB; (m) CJ wild-type centered at N182 and (n) N182C. After installation at N182C: (o) Two 50%-occupancy conformations for MBO. (p) One 100%-occupancy conformation for MNB. (q) One fully resolved 100%-occupancy conformation for SEC. (r) One 90%-occupancy conformation for MBB.

Discussion

Of the attempted structure determination targets, only one cysteine:adduct pair (mBBr installation at G34C) has yet to yield interpretable electron density for the guest molecule. Notably, G34C crystals became highly fluorescent when incubated with mBBr. We therefore speculate that installation succeeded, but the resulting adduct was too mobile to be clearly resolved in the electron density map. It is not uncommon for surface sidechain

disorder to lead to ambiguous or absent electron density contours (e.g. Lys46 and Lys50 in Figure 2).

Subtle conformational changes on the scaffold surface were observed upon small molecule installation. The least subtle example was N156. The apparent native hydrogen bond network (Figure 2m) was disrupted upon mutating N182C. For the N182C model, we placed N156 to accept a hydrogen bond from S154 (Figure 2n). N156 moved again when small molecules were installed at the N182C site, to avoid steric clashes (Figures 2p, q, and r) or to make favorable interactions with the adduct (Figure 2o).

As is typical for protein crystals, many surface sidechains were too disordered to be easily placed in electron density (15 out of 180 sidechains were truncated). *A priori*, it was not clear if small molecule adducts would be likely to adopt ordered conformations, especially considering the absence of any design or selection pressure. Indeed, adducts were quite flexible, leading to high B-factors (Tables S1-S5). Despite high B-factors, the high real-space correlation coefficients for the modeled guest molecules (Table 1) and omit map analysis (Figures S15, S16, and S17) suggested that the molecules were correctly modeled.

To analyze ligand flexibility, the average B-factor for each conjugation product was plotted as a function of bond count from the alpha-carbon (Figure S20-S23). For highly flexible conjugates, it might be expected that the B-factor would dramatically increase the further from the attachment point. In contrast, for our well-resolved adducts (real space correlation coefficient >90%) there was only a modest increase in B-factor beyond the attachment SG atom. Counterintuitively, for the lower quality conjugate structures the B-factor profile resembled a step function. A significant B-factor increase is observed at the first ligand atom followed by a relatively flat profile. Additionally, this analysis revealed that B-factors for G34C structures were consistently higher than the other structures. The trend is particularly obvious when comparing the B-factors for the cysteine sulfur atom (SG). The high flexibility of G34C atoms correlates with the poorly resolved ligands at G34C.

In theory, we could use anomalous diffraction to gather more information on the position of selenium and mercury atoms. However, anomalous scattering would be more useful if the atoms in question were not directly attached to the cysteine and were not already evident due to dramatic electron density features. Ideally, scaffold assisted crystallography will not require anomalous scattering sites. Such sites are not required for the current effort to determine how and when adduct molecules adopt coherent structures.

This study supports our original supposition that limiting conformational flexibility is pivotal to resolving guest molecules via scaffold-assisted crystallography. We only observed guest molecules at the intended covalent installation sites. Additionally, the most readily resolved guest small molecule was MNB. It seems likely that the observed coherent MNB conformations were adopted due to the preferred geometry of the disulfide dihedral (86.1° and 85.9° for N48C and N182C respectively) and the rigidity of the subsequent planar ring structure. In contrast, molecules with multiple rotatable bonds such as SEC more often yielded poorly resolved structures past the initial attachment point. We are currently investigating the use of chemical crosslinking to stabilize the host crystals, thereby enabling diffraction under widely varying solution conditions and cryoprotectants. Varying the solution conditions may ultimately resolve multiple coherent guest conformations.

While the modest resolution of CJ crystals (>2.4 Å) is not ideal for high-resolution structure determination of installed small molecules, a major long-term advantage of developing the CJ crystal platform is the promise of scalability to large guest molecules. The techniques developed herein could be adapted to protein crystals with higher resolution, which might result in more detailed adduct structures. However, increased crystal resolution will not necessarily improve adduct detail. Ueno, studying myoglobin crystal adducts (installed prior to crystallization) found little interpretable density despite the superior resolution of myoglobin crystals (~1.5 Å).[29]

More likely, the current work suggests that variation of installation sites, optimization of neighboring amino acids, and perhaps provision of strong secondary anchoring interactions, will be key to fully realizing guest molecule structure determination. Ni and Tezcan demonstrated the importance of secondary interactions in resolving an unknown microperoxidase using a crystalline protein cage as a scaffold.[47] In this study, installation sites were purposely selected to be highly exposed and proximal to the 13 nm axial solvent channels. Despite a lack of designed secondary interactions, we were able to model adducts at high occupancy and high B-factor (Table S1-S5). Clear patterns emerged, in that one site (N182C) led to more coherent adduct structures than another site (G34C). Future small molecule adduct structure determination may be improved if installation sites are partially buried in a surface pocket. Less accessible installation sites might reduce adduct flexibility, though perhaps conjugation efficiency could suffer. Additionally, engineering the environment near the installation sites may increase success in determining coherent structures. For example, mutagenesis of neighboring amino acids to hydrophobic side chains might promote favorable interactions with some guest molecules. Ultimately, the plasticity of the protein crystal makes this system an evolvable platform for scaffold-assisted crystallography.

Table 1. Summary of Small Molecule Guest Installation Results and Deposited Structures

		MBO	MNB	SEC	MBB
G34C	Number of States	1	1	2	-
	Occupancy	90%	100%	50%/50%	
	Real Space cc	0.89	0.75	0.93/0.92	-
	Notes	Hg atom only	Fully resolved	Se atom only	Small peak unresolved
	PDB Code	5W2K	5W2R	5W2V	-
N48C	Number of States	1	1	1	1
	Occupancy	85%	100%	90%	100%
	Real Space cc	0.99	0.85	0.81	0.90
	Notes	Fully Resolved	Fully resolved	Se and alpha carbon only	Fully Resolved
	PDB Code	5W31	5W2Z	5W32	5W30
N182C	Number of States	2	1	1	1
	Occupancy	50%/50%	100%	100%	90%
	Real Space cc	0.98/0.86	0.90	0.95	0.87
	Notes	Multiple states, complex	Fully resolved	Fully resolved	Fully Resolved
	PDB Code	5W3B	5W3A	5W3C	5W39

*Real space cc calculated from 2mFo-DFc map using Phenix.

Conclusions

We have demonstrated that several established thiol conjugation strategies are suitable for installing small molecules upon engineered cysteines in a pre-existing three-dimensional protein crystal. This strategy enables diverse nanotechnological applications. The visibility of the resulting small molecule conjugates is promising for advancing techniques in scaffold-assisted crystallographic structure determination. The conjugation strategies demonstrated here could be adapted to conjugate small molecules of unknown structure to alternate protein crystal scaffolds with superior resolution and engineered local

environment to promote favorable guest-scaffold contacts. Alternately, in contrast to the MOFs currently used for guest structure determination,[24,26] the 13-nm pores of CJ crystals used here are large enough to accommodate macromolecules such as proteins, inorganic nanoparticles, and DNA. The methods developed herein lay the groundwork for site-specific installation of macromolecules and structure determination of the resulting co-crystals.

Methods

CJ Protein Crystal Preparation

A codon optimized gene encoding a putative periplasmic protein (Genebank ID: cj0420) from *Campylobacter jejuni* was obtained from Life Technologies and cloned into pSB3 vector at NdeI and XhoI. For cytosolic expression, the gene was truncated to remove the signaling peptide. Thiol variants were generated via single primer mutagenesis with Q5 polymerase (New England Biolabs) and sequenced verified. All variants were expressed in *E. coli* C41 (DE3) (Lucigen) grown in Terrific Broth and induced with 0.4 mM IPTG at 25 °C for 16 hr. The cells were harvested and sonicated into a lysis buffer (50 mM HEPES, 500 mM NaCl, 10% glycerol, 25 mM imidazole, pH 7.4). The lysate was clarified and purified via Ni^{2+}-NTA chromotagraphy (Thermo Fisher Scientific HisPur™ Ni-NTA). A single chromatography step provided sufficient purity for crystallization. The purified protein was dialyzed into a storage buffer (10 mM HEPES, 500 mM $(NH_4)_2SO_4$, 10% glycerol at pH 7.4), aliquoted, and stored at -20 °C. The final concentration was ~20 mg/mL with an average CJ yield of >100 mg per 1 L culture. CJ variants were crystallized overnight by sitting drop vapor diffusion at 20 °C in >3.0 M $(NH_4)_2SO4$, 0.1 M Bis-Tris pH 6.0.
Prior to installation, crystals were washed via transfer to the installation solution (3.4 M $(NH_4)_2SO4$, 100 mM HEPES, pH 7.5) for 15 min to equilibrate the crystals and remove excess free protein. Crystals were then transferred to 20 μL of the installation solution with 500 μM of the molecule to be conjugated and incubated for 2 hours.

X-Ray Diffraction and Data Processing

In all cases, individual crystals were briefly swished through a cryoprotectant solution containing 3.2 M $(NH_4)_2SO4$ and either 10% glycerol or 10% ethylene glycol at pH 7.5 and flash frozen in liquid nitrogen. X-ray diffraction data was collected on beamline 4.2.2 at the Advanced Light Source (ALS) or on a local Rigaku Compact HomeLab with a microfocus X-ray generator and a Pilatus 200K detector. The collected data was processed with XDS.[48] The wild-type structure was determined by molecular replacement (MR) with the Campylobacter jejuni putative periplasmic protein (PDB entry 2fgs) as a search model. Model refinement was performed in COOT using sigma weighted ($2mF_o$-DF_c) and (mF_o-DF_c) electron density maps and REFMAC5 from the CCP4 suite.[49–51] The resulting wild-type model was used as the starting MR model for G34C, N48C, and N182C with the same refinement scheme. Each cysteine variant model was then used as a MR search model for their corresponding small molecule adducts. The molecular refinement workflow is summarized in Figure S12. For each thiol structure with an installed small molecule, a scheme of discovery map generation, ligand building, refinement, and omit map generation was implemented to reduce model bias. The model building scheme is summarized in Figure S13.

Conflicts of interest

There are no conflicts to declare.

Acknowledgements

Jay Nix at Beamline 4.2.2 at Advanced Light Source (ALS), Crystal Vander Zanden in the Biochemistry at Colorado State University for maintaining Rigaku Homelab. This material is based upon work supported by the National Science Foundation under Grant Numbers 1434786, 1506219, and 1645015. Funding for shared facilities used in this research was provided by an NSF MRI 1531921.

Supporting Information

Experimental methods, Figures S1-S17, and Table S1-S6. The Supporting Information is available free of charge on the ACS Publications website.

5W17.cif (CJ without thiol), **5W2D**.cif (CJ-G34C), **5W2K**.cif (CJ-G34C-MBO), **5W2R**.cif (CJ-G34C-MNB), **5W2V**.cif (CJ-G34C-SEC), **5W2X**.cif (CJ-N48C), **5W31**.cif (CJ-N48C-MBO), **5W2Z**.cif (CJ-N48C-MNB), **5W32**.cif (CJ-N48C-SEC), **5W30**.cif (CJ-N48C-MBB), **5W37**.cif (CJ-N182C), **5W3B**.cif (CJ-N182C-MBO), **5W3A**.cif (CJ-N182C-MNB), **5W3C**.cif (CJ-N182C-SEC), **5W39**.cif (CJ-N182C-MBB)

References

(1) Pandya, M. J., Spooner, G. M., Sunde, M., Thorpe, J. R., Rodger, A., and Woolfson, D. N. (2000) Sticky-end assembly of a designed peptide fiber provides insight into protein fibrillogenesis. *Biochemistry (Mosc.) 39*, 8728–8734.
(2) Potekhin, S. A., Melnik, T. N., Popov, V., Lanina, N. F., Vazina, A. A., Rigler, P., Verdini, A. S., Corradin, G., and Kajava, A. V. (2001) De novo design of fibrils made of short alpha-helical coiled coil peptides. *Chem. Biol. 8*, 1025–1032.
(3) Ogihara, N. L., Ghirlanda, G., Bryson, J. W., Gingery, M., DeGrado, W. F., and Eisenberg, D. (2001) Design of three-dimensional domain-swapped dimers and fibrous oligomers. *Proc. Natl. Acad. Sci. U. S. A. 98*, 1404–1409.
(4) Papapostolou, D., Smith, A. M., Atkins, E. D. T., Oliver, S. J., Ryadnov, M. G., Serpell, L. C., and Woolfson, D. N. (2007) Engineering nanoscale order into a designed protein fiber. *Proc. Natl. Acad. Sci. 104*, 10853–10858.
(5) Padilla, J. E., Colovos, C., and Yeates, T. O. (2001) Nanohedra: using symmetry to design self assembling protein cages, layers, crystals, and filaments. *Proc. Natl. Acad. Sci. U. S. A. 98*, 2217–2221.
(6) Lai, Y.-T., Cascio, D., and Yeates, T. O. (2012) Structure of a 16-nm Cage Designed by Using Protein Oligomers. *Science 336*, 1129–1129.
(7) King, N. P., Sheffler, W., Sawaya, M. R., Vollmar, B. S., Sumida, J. P., Andre, I., Gonen, T., Yeates, T. O., and Baker, D. (2012) Computational Design of Self-Assembling Protein Nanomaterials with Atomic Level Accuracy. *Science 336*, 1171–1174.
(8) King, N. P., Bale, J. B., Sheffler, W., McNamara, D. E., Gonen, S., Gonen, T., Yeates, T. O., and Baker, D. (2014) Accurate design of co-assembling multi-component protein nanomaterials. *Nature 510*, 103–108.
(9) Lai, Y.-T., Reading, E., Hura, G. L., Tsai, K.-L., Laganowsky, A., Asturias, F. J., Tainer, J. A., Robinson, C. V., and Yeates, T. O. (2014) Structure of a designed protein cage that self-assembles into a highly porous cube. *Nat. Chem. 6*, 1065.

(10) Bale, J. B., Gonen, S., Liu, Y., Sheffler, W., Ellis, D., Thomas, C., Cascio, D., Yeates, T. O., Gonen, T., King, N. P., and Baker, D. (2016) Accurate design of megadalton-scale two-component icosahedral protein complexes. *Science 353*, 389–394.
(11) Hsia, Y., Bale, J. B., Gonen, S., Shi, D., Sheffler, W., Fong, K. K., Nattermann, U., Xu, C., Huang, P.-S., Ravichandran, R., Yi, S., Davis, T. N., Gonen, T., King, N. P., and Baker, D. (2016) Design of a hyperstable 60-subunit protein dodecahedron. [corrected]. *Nature 535*, 136–139.
(12) Douglas, T., and Young, M. (2006) Viruses: Making Friends with Old Foes. *Science 312*, 873–875.
(13) Lee, S.-Y., Lim, J.-S., and Harris, M. T. (2012) Synthesis and application of virus-based hybrid nanomaterials. *Biotechnol. Bioeng. 109*, 16–30.
(14) Chen, Z., Li, N., Li, S., Dharmarwardana, M., Schlimme, A., and Gassensmith, J. J. (2016) Viral chemistry: the chemical functionalization of viral architectures to create new technology. *Wiley Interdiscip. Rev. Nanomed. Nanobiotechnol. 8*, 512–534.
(15) Moll, D., Huber, C., Schlegel, B., Pum, D., Sleytr, U. B., and Sára, M. (2002) S-layer-streptavidin fusion proteins as template for nanopatterned molecular arrays. *Proc. Natl. Acad. Sci. 99*, 14646–14651.
(16) Sleytr, U. B., Egelseer, E. M., Ilk, N., Pum, D., and Schuster, B. (2007) S-Layers as a basic building block in a molecular construction kit. *FEBS J. 274*, 323–334.
(17) Baneyx, F., and Matthaei, J. F. (2014) Self-assembled two-dimensional protein arrays in bionanotechnology: from S-layers to designed lattices. *Curr. Opin. Biotechnol. 28*, 39–45.
(18) Margolin, A. L., and Navia, M. A. (2001) Protein Crystals as Novel Catalytic Materials. *Angew. Chem. Int. Ed. 40*, 2204–2222.
(19) Wei, H., Wang, Z., Zhang, J., House, S., Gao, Y.-G., Yang, L., Robinson, H., Tan, L. H., Xing, H., Hou, C., Robertson, I. M., Zuo, J.-M., and Lu, Y. (2011) Time-dependent, protein-directed growth of gold nanoparticles within a single crystal of lysozyme. *Nat. Nanotechnol. 6*, 93–97.
(20) Abe, S., Tsujimoto, M., Yoneda, K., Ohba, M., Hikage, T., Takano, M., Kitagawa, S., and Ueno, T. (2012) Porous Protein Crystals as Reaction Vessels for Controlling Magnetic Properties of Nanoparticles. *Small 8*, 1314–1319.
(21) England, M. W., Lambert, E. M., Li, M., Turyanska, L., Patil, A. J., and Mann, S. (2012) Fabrication of polypyrrole nano-arrays in lysozyme single crystals. *Nanoscale 4*, 6710–6713.
(22) Lanci, C. J., MacDermaid, C. M., Kang, S., Acharya, R., North, B., Yang, X., Qiu, X. J., DeGrado, W. F., and Saven, J. G. (2012) Computational design of a protein crystal. *Proc. Natl. Acad. Sci. 109*, 7304–7309.
(23) Maity, B., Abe, S., and Ueno, T. (2017) Observation of gold sub-nanocluster nucleation within a crystalline protein cage. *Nat. Commun. 8*, 14820.
(24) Inokuma, Y., Yoshioka, S., Ariyoshi, J., Arai, T., Hitora, Y., Takada, K., Matsunaga, S., Rissanen, K., and Fujita, M. (2013) X-ray analysis on the nanogram to microgram scale using porous complexes. *Nature 495*, 461–466.
(25) Ledford, H. (2015) Controversial molecular-analysis tool tries for a comeback. *Nature*.
(26) Lee, S., Kapustin, E. A., and Yaghi, O. M. (2016) Coordinative alignment of molecules in chiral metal-organic frameworks. *Science 353*, 808–811.
(27) McElroy, H. E., Sisson, G. W., Schoettlin, W. E., Aust, R. M., and Villafranca, J. E. (1992) Studies on engineering crystallizability by mutation of surface residues of human thymidylate synthase. *J. Cryst. Growth 122*, 265–272.

(28) D'Arcy, Stihle, M., Kostrewa, D., and Dale, G. (1999) Crystal engineering: a case study using the 24 kDa fragment of the DNA gyrase B subunit from Escherichia coli. *Acta Crystallogr. D Biol. Crystallogr. 55*, 1623–1625.
(29) Koshiyama, T., Kawaba, N., Hikage, T., Shirai, M., Miura, Y., Huang, C.-Y., Tanaka, K., Watanabe, Y., and Ueno, T. (2010) Modification of porous protein crystals in development of biohybrid materials. *Bioconjug. Chem. 21*, 264–269.
(30) Forsythe, E., Achari, A., and Pusey, M. L. (2006) Trace fluorescent labeling for high-throughput crystallography. *Acta Crystallogr. D Biol. Crystallogr. 62*, 339–346.
(31) Huber, T. R., Hartje, L. F., McPherson, E. C., Kowalski, A. E., and Snow, C. D. (2016) Programmed Assembly of Host–Guest Protein Crystals. *Small* 10.1002/smll.201602703.
(32) Kowalski, A. E., Huber, T. R., Ni, T. W., Hartje, L. F., Appel, K. L., Yost, J. W., Ackerson, C. J., and Snow, C. D. (2016) Gold nanoparticle capture within protein crystal scaffolds. *Nanoscale 8*, 12693–12696.
(33) Hermanson, G. T. (2013) Bioconjugate Techniques. Academic Press.
(34) Pike, A. C. W., Garman, E. F., Krojer, T., von Delft, F., and Carpenter, E. P. (2016) An overview of heavy-atom derivatization of protein crystals. *Acta Crystallogr. Sect. Struct. Biol. 72*, 303–318.
(35) Sun, D. P., Alber, T., Bell, J. A., Weaver, L. H., and Matthews, B. W. (1987) Use of site-directed mutagenesis to obtain isomorphous heavy-atom derivatives for protein crystallography: cysteine-containing mutants of phage T4 lysozyme. *Protein Eng. 1*, 115–123.
(36) Ellman, G. L. (1959) Tissue sulfhydryl groups. *Arch. Biochem. Biophys. 82*, 70–77.
(37) Riddles, P. W., Blakeley, R. L., and Zerner, B. (1983) Reassessment of Ellman's reagent. *Methods Enzymol. 91*, 49–60.
(38) Winther, J. R., and Thorpe, C. (2014) Quantification of Thiols and Disulfides. *Biochim. Biophys. Acta 1840*.
(39) Beld, J., Woycechowsky, K. J., and Hilvert, D. (2010) Diselenides as universal oxidative folding catalysts of diverse proteins. *J. Biotechnol. 150*, 481–489.
(40) Steinmann, D., Nauser, T., and Koppenol, W. H. (2010) Selenium and Sulfur in Exchange Reactions: A Comparative Study. *J. Org. Chem. 75*, 6696–6699.
(41) Sardi, F., Manta, B., Portillo-Ledesma, S., Knoops, B., Comini, M. A., and Ferrer-Sueta, G. (2013) Determination of acidity and nucleophilicity in thiols by reaction with monobromobimane and fluorescence detection. *Anal. Biochem. 435*, 74–82.
(42) Tronrud, D. (2014, November 14) [phenixbb] simulated annealing omit map.
(43) Afonine, P. V., Moriarty, N. W., Mustyakimov, M., Sobolev, O. V., Terwilliger, T. C., Turk, D., Urzhumtsev, A., and Adams, P. D. (2015) FEM: feature-enhanced map. *Acta Crystallogr. D Biol. Crystallogr. 71*, 646–666.
(44) Liebschner, D., Afonine, P. V., Moriarty, N. W., Poon, B. K., Sobolev, O. V., Terwilliger, T. C., and Adams, P. D. (2017) Polder maps: improving OMIT maps by excluding bulk solvent. *Acta Crystallogr. Sect. Struct. Biol. 73*, 148–157.
(45) Hodel, A., Kim, S.-H., and Brünger, A. T. (1992) Model bias in macromolecular crystal structures. *Acta Crystallogr. A 48*, 851–858.
(46) Adams, P. D., Afonine, P. V., Bunkóczi, G., Chen, V. B., Davis, I. W., Echols, N., Headd, J. J., Hung, L.-W., Kapral, G. J., Grosse-Kunstleve, R. W., McCoy, A. J., Moriarty, N. W., Oeffner, R., Read, R. J., Richardson, D. C., Richardson, J. S., Terwilliger, T. C., and Zwart, P. H. (2010) PHENIX: a comprehensive Python-based system for macromolecular structure solution. *Acta Crystallogr. D Biol. Crystallogr. 66*, 213–221.

(47) Structural Characterization of a Microperoxidase Inside a Metal-Directed Protein Cage - Ni - 2010 - Angewandte Chemie International Edition - Wiley Online Library.
(48) Kabsch, W. (2010) XDS. *Acta Crystallogr. D Biol. Crystallogr. 66*, 125–132.
(49) Emsley, P., Lohkamp, B., Scott, W. G., and Cowtan, K. (2010) Features and development of Coot. *Acta Crystallogr. D Biol. Crystallogr. 66*, 486–501.
(50) Winn, M. D., Ballard, C. C., Cowtan, K. D., Dodson, E. J., Emsley, P., Evans, P. R., Keegan, R. M., Krissinel, E. B., Leslie, A. G. W., McCoy, A., McNicholas, S. J., Murshudov, G. N., Pannu, N. S., Potterton, E. A., Powell, H. R., Read, R. J., Vagin, A., and Wilson, K. S. (2011) Overview of the CCP4 suite and current developments. *Acta Crystallogr. D Biol. Crystallogr. 67*, 235–242.
(51) Vagin, A. A., Steiner, R. A., Lebedev, A. A., Potterton, L., McNicholas, S., Long, F., and Murshudov, G. N. (2004) REFMAC5 dictionary: organization of prior chemical knowledge and guidelines for its use. *Acta Crystallogr. D Biol. Crystallogr. 60*, 2184–2195.

TABLE OF CONTENTS FIGURE

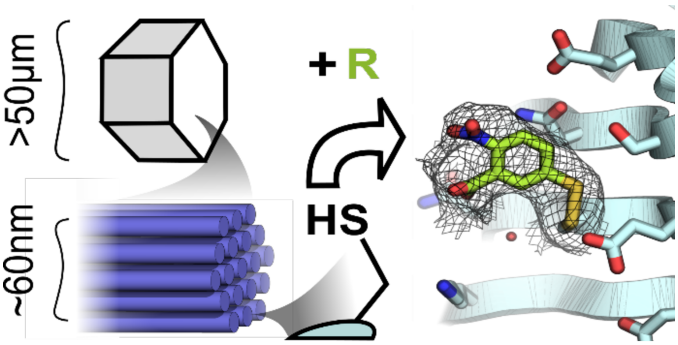

Structure determination of guest molecules using scaffold assisted crystallography with an evolvable porous protein crystal.